

**STRUCTURAL AND OPTICAL STUDIES OF a-Si:H THIN FILMS:
FROM AMORPHOUS TO NANOCRYSTALLINE SILICON¹****J. Müllerová^{a,2}, S. Jurečka^a, P. Šutta^b, M. Mikula^c**^a *Department of Engineering Fundamentals, Faculty of Electrical Engineering,
University of Žilina, 031 01 Liptovský Mikuláš, Slovakia*^b *University of West Bohemia, New Technologies – Research Centre,
Univerzitní 8, 306 14 Plzeň, the Czech Republic*^c *Department of Graphic Arts Technology and Applied Photochemistry, Faculty of Chemical
and Food Technology, Slovak Technical University, Radlinského 9, 812 37 Bratislava, Slovakia*

Received 11 February 2005, accepted 25 February 2005

We report on the results of the investigation of surface morphology, structure and optical properties of plasma deposited thin films of hydrogenated amorphous silicon determined by atomic force microscopy, X-ray diffraction and UV-Vis and IR spectroscopy. The influence of the both hydrogen dilution of silane plasma in the plasma deposition and the film thickness on the film properties was investigated. The structure, the refractive index and the optical band gap of the dilution series and the thickness series were analyzed. The changes are discussed and correlated with the changes of the surface morphology and the hydrogen to silicon bonding. The results show that at dilution of ~ 30 the transition from amorphous to crystalline phase occurs and the sample becomes a mixture of amorphous phase, polycrystalline phase with nano-sized grains and voids. The optical band gap becomes larger than that of the undiluted sample.

PACS: 68.55 Jk, 78.66 Jg, 81.05 Gc, 81.15 Gh

1 Introduction

Unique properties of hydrogenated amorphous silicon (a-Si:H) such as the high light absorption, lower defect density when compared with amorphous Si, the low temperature for deposition ($< 250^\circ\text{C}$) on low cost substrates (glass, metals, plastics) favouring the growth of good quality materials, make the material attractive for applications of considerable industrial interest, e.g. in photovoltaics, electrophotographics, thin film light emitting diodes, photosensors, thin film transistors etc.

It is known that Si:H thin film properties depend significantly on the deposition conditions. Therefore, structural properties, hydrogen content, voids, optical and electrical properties have

¹Presented at SSSI-IV (Solid State Surfaces and Interfaces IV) Conference, Smolenice, Slovakia, 8–11 Nov. 2004.²E-mail address: mullerova@lm.utc.sk

been analysed intensively. However, this dependence offers the possibility of tailoring processing parameters to deposit a film with specific properties.

In thin film solar technologies based on a-Si:H the extensive and continuing research on improving efficiency and resistance to light-induced degradation (Staebler - Wronski effect [1]) is evident. One of the most popular chemistries for Si film deposition is the plasma-enhanced chemical vapour deposition (PECVD) with hydrogen (H_2) dilution of silane (SiH_4) plasma reported as improving both material and solar cell stability. The films prepared at the amorphous-to-crystalline phase boundary consisting of small crystallites of 10 ~100 nm embedded in a-Si network are recommended for manufacturing more stable solar cells [1–3].

The paper reports on the properties of Si:H thin films deposited on glass by PECVD under various hydrogen dilution. The results of surface morphology studies by atomic force microscopy (AFM), X-ray diffraction (XRD), UV-Vis and IR spectrophotometry are presented. The effect of H_2 dilution of SiH_4 and of the film thickness on film properties is under discussion.

2 Experimental

The samples of undoped a-Si:H were PECVD deposited at the Delft University of Technology, the Netherlands [4], by the industrial rf 13.56 MHz excited parallel plate ($15 \times 15 \text{ cm}^2$) deposition system from H_2 diluted SiH_4 plasma on Corning 1737 glass substrate. Other deposition parameters were kept constant (substrate temperature 194°C , total chamber pressure 200 Pa, rf power 13.5 W) to avoid their affecting the film properties. The dilution D is a non-dimensional quantity defined as the ratio of H_2/SiH_4 gas flows. Besides this deposition parameter, also SiH_4 concentration defined as the ratio of $SiH_4 / (H_2 + SiH_4)$ gas flows is often used. The dilution series with approximately the same thickness and thickness series deposited at the same dilution were investigated (Table 1).

The surface morphology was investigated by the atomic force microscope NT - MDT SPM Solver P7 LS measuring in air in the contact repulsive mode using a silicon tip cantilever. The lateral resolution of AFM measurements was $\sim 1 - 2$ nm, the vertical resolution 0.01 nm. XRD analysis was carried out with an X-ray diffractometer Bruker AXS D8 with a 2D detector using $CoK\alpha$ radiation ($\lambda_{CoK\alpha} = 0.179021$ nm). The XRD patterns were collected by setting the detec-

Tab. 1. The description of the samples under study.

dilution series				thickness series			
sample	dilution D	SiH_4 concentration	thickness [nm]	sample	dilution D	SiH_4 concentration	thickness [nm]
A 1375	0	100	390	A1380	20	4.8	98
A 1374	10	9.1	394	A 1379	20	4.8	198
A 1370	20	4.8	385	A1378	20	4.8	302
A 1371	30	3.2	388	A 1370	20	4.8	385
A 1399	40	2.4	402				
A 1400	50	2.0	397				

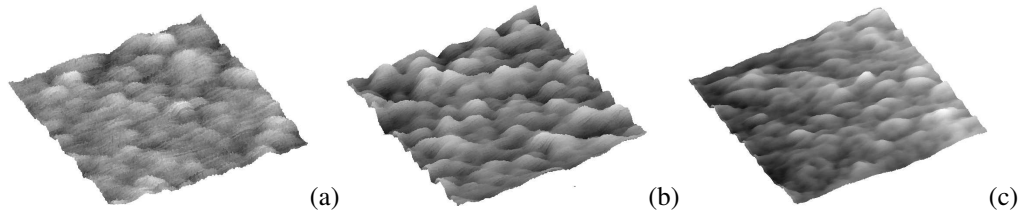


Fig. 1. AFM image of the sample (a) A 1374 ($D = 10$), (b) A 1371 ($D = 30$), and (c) A 1400 ($D = 50$). Scanning area is $2 \times 2 \mu\text{m}^2$.

tor position at 30 deg and 55 deg of 2ϑ , with a counting time of 20 seconds at each position. The sample – detector distance was set up to 15 cm.

UV-Vis transmittance and reflectance spectral measurements were performed with Pye Unicam/Philips PU 8800 spectrophotometer in the double beam mode and the spectral region (300 – 900) nm with 2 nm slit at nearly normal incidence and at room temperature. The probed sample areas were $\sim 0.2 \text{ cm}^2$. A freshly evaporated aluminium sample was used for the reference reflectance data collection. FTIR - DIGILAB FTS 3000MX Excalibur spectrophotometer in the internal HATR (horizontal attenuated total reflection) mode with ZnSe crystal and 7 multiple reflections was used to measure the infrared spectral absorbance.

3 Results

3.1 Surface morphology

Contact mode AFM surface analysis of the sample frames $2 \times 2 \mu\text{m}^2$ shows microcrystalline features appearing on the surface with increasing dilution as can be seen in the 3D AFM images in Figs. 1(a), 1(b), and 1(c). The visual inspection of AFM images indicates the isotropic surfaces with no textures and no directions related to the surface roughness.

As AFM can sense vertical deviations of the sample surface vertical relief structure can be determined from AFM data by the calculation of the average roughness (arithmetic mean surface roughness) and rms roughness (root-mean-square roughness) (Figs. 2, 3). The rms and average roughness in the dilution series (Fig. 2) show the maximum at $\sim D = 30$ at which for the samples under study the amorphous-to-crystalline transition may be expected. This increase may be connected with growing crystalline grains according to the geometrical model of conical microcrystalline conglomerates [4, 5]. The thin film prepared at this dilution may be considered as the film on the boundary between amorphous and crystalline phase. The lateral dimensions of the largest features are $\sim 200 \text{ nm}$ for the films prepared at $D = 30$ (Fig. 1(b)) and they are separated by amorphous tissue. With D increasing over this value the lateral size of grains decreases ($\sim 100 \text{ nm}$ for the samples A 1399, A 1400 at $D = 40$, $D = 50$), they finally touch to form smoother surface (Fig. 1(c)) resembling visually the amorphous sample (e.g. Fig. 1(a)).

In the thickness series (Fig. 3) the depth of features according to average and rms roughness decreases slightly with increasing thickness being under 1.5 nm for all members of the series. The crystalline grain growth seems to be negligible at $D = 20$ in spite of increasing thickness

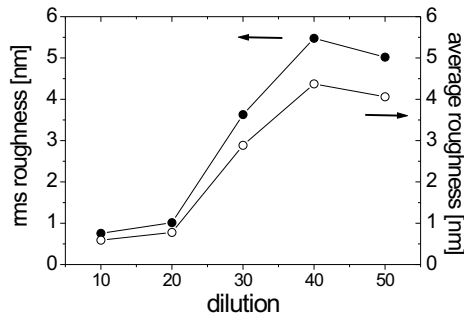


Fig. 2. Average and rms roughness of the dilution series.

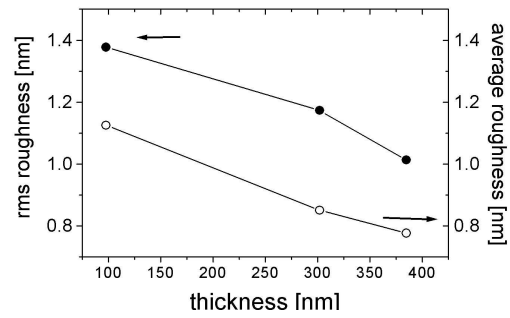


Fig. 3. Average and rms roughness of the thickness series.

of the films up to ~ 400 nm. For all samples under study the rms roughness does not exceed the value of ~ 6 nm.

3.2 Structure analysis

XRD scans of the first three members of the dilution series at $D < 30$ show no diffraction lines of crystalline Si. We conclude that the samples are either amorphous or with negligible part of the crystalline phase. The XRD scans of the samples of the dilution series at $D \geq 30$ are in Fig. 4 and show the evolution of three diffraction lines. These predominant peaks are ascribed to (111), (220), and (311) planes of crystalline silicon structure suggesting that the films become polycrystalline silicon (polysilicon). For the comparison the XRD scan of the amorphous glass substrate is added to the plot in Fig. 4. The XRD scans of the thickness series (Fig. 5) resemble the scan of the glass substrate with no apparent presence of the crystalline phase.

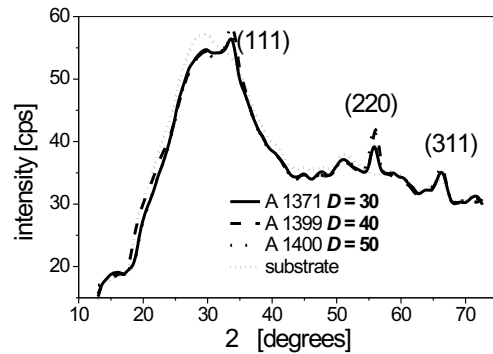


Fig. 4. XRD scans of the dilution series samples prepared at $D \geq 30$ and of the glass substrate.

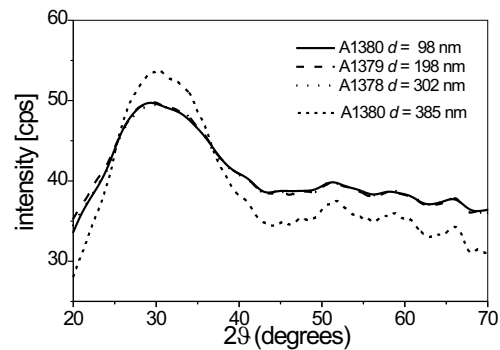


Fig. 5. XRD scans of the thickness series samples prepared at the same dilution $D = 20$.

Tab. 2. Residual stress – macrostress and microstrain.

sample	dilution D	diffraction	line [deg]	position	grain size [nm]	average microstrain
A 1371	30	33.73	55.88	66.23	10 ± 3	0.02
A 1399	40	34.16	56.09	66.19	10 ± 3	0.02
A 1400	50	33.63	55.81	66.25	40 ± 5	0.005
standard		33.15	55.28	66.25		
biaxial stress		tensile	tensile	compressive		

Owing to the crystalline lines detected in the diffractograms, the samples A 1371, A 1399 and A 1400 deserve further analysis considering residual stresses in the films by the procedures outlined in [7]. From the shift of the diffraction lines in consideration to the position of the standard diffraction lines, the biaxial lattice stress (so-called macrostress) was calculated (Table 2). The reference interplanar spacings were calculated “ab initio” from the structure model for the strain free state. From the broadening of diffraction lines the average microstrain (relative microdeformation) and the average size of the coherently diffracting domains can be deduced. The size of the coherently diffracting domains or simply the grain size is defined as the average size of crystallites perpendicular to the diffracting plane. For the calculations, ceramic Al_2O_3 from NIST (National Institute for Standards and Technology) was used as an instrumental standard.

The size of crystalline grains determined from the XRD analysis (Table 2) is much smaller than that of surface features inspected by AFM measurements. We can conclude that features seen by AFM are aggregates of nanocrystalline grains detected by the XRD analysis for the samples prepared at $D \geq 30$ (A 1371, A 1399, A 1400).

Obviously, these samples become mixed phase films also according to the Raman spectra [8]. We calculated the ratio $x_c = I_{520}/(I_{520} + I_{480})$ of the maximum intensities of the Raman peaks at 520 cm^{-1} belonging to the crystalline Si and that at 480 cm^{-1} of amorphous Si. This quantity is considered as a figure of merit of the degree of the film crystallinity. For our dilution series, the degree of crystallinity increases with increasing dilution as follows: $x_c = 0 \%$ ($D = 0$), $x_c = 61 \%$ ($D = 30$), $x_c = 73 \%$ ($D = 40$), $x_c = 82 \%$ ($D = 50$). Thus, Raman spectra provide the same observation of the progressive formation of crystalline Si with increasing D as AFM and XRD data.

3.3 Optical properties

We studied the effect of the structure on the optical properties of the dilution and thickness series. For the determination of optical properties – the refractive index and the Tauc’s optical band gap - the model of a quasi-ideal single homogeneous layer with the thickness d with smooth parallel interfaces on the thick incoherent substrate was used.

The spectral reflectance and transmittance are non-linear functions of optical properties and the wavelength [9]. They were compared with the experimental data by the optimization method based on the genetic algorithm optimisation procedure VIMSO [10]. by point to-point processing without any dispersion model with the aim to determine the optical properties. Spectral refractive

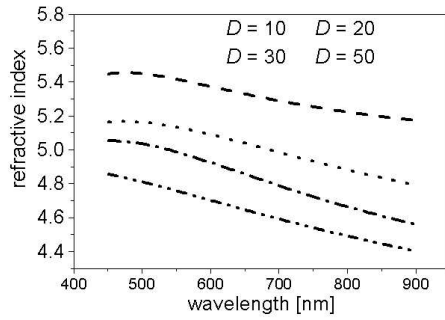


Fig. 6. Refractive indices of the dilution series. The film prepared at $D = 40$ reveals approx. the same spectral refractive index as the film at $D = 50$.

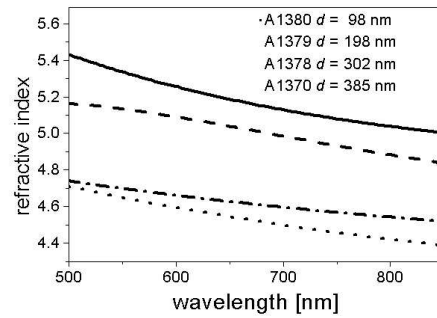


Fig. 7. Refractive indices of the thickness series.

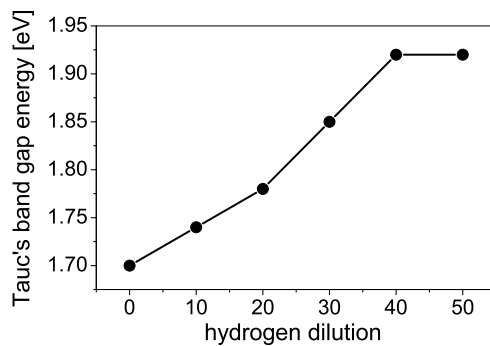


Fig. 8. Optical band gap versus the dilution.

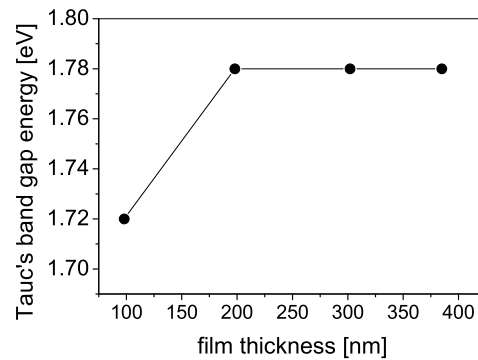


Fig. 9. Optical band gap versus the film thickness.

indices of the dilution and the thickness series are in Figs. 6, 7. The refractive index decreases with increasing dilution therefore we deduce that the density of films prepared at higher dilution decreases. This may be probably due to the voids - sites with missing radicals of $\text{SiH}_4 - \text{H}_2$ decomposition.

The values of the optical band gap energy E_g were found from Tauc's plot [plot of $(\alpha E)^{1/2}$ versus photon energy E extrapolated to zero absorption]. The absorption coefficient α was deduced from transmittance spectra in the vicinity of to the absorption edge in the interference free zone. Fig. 8 shows the relationship between the optical band gap and the dilution, Fig. 9 the relationship between E_g and the film thickness. More significant change of the optical bad gap was found as a function of the dilution than as a function of the film thickness. The band gap appears to increase with increasing D . As can be seen in Fig. 8, the dilution opens the optical band gap with respect to non-diluted film of about 0.25 eV. Besides this, similar optical proper-

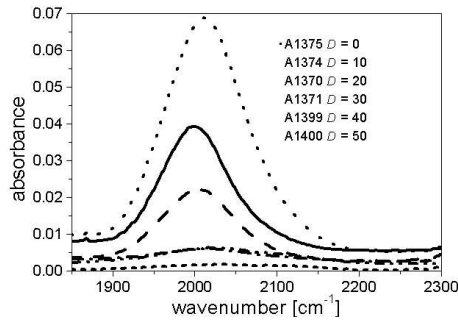


Fig. 10. Vibrational absorption peaks of the dilution series.

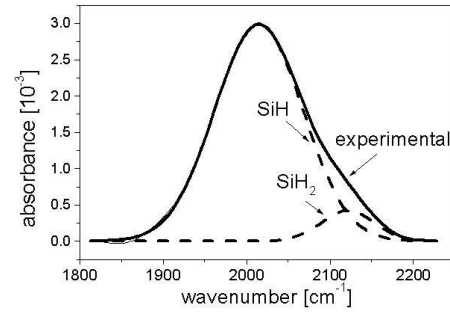


Fig. 11. Deconvolution of the vibrational absorption peaks of the sample A 1371 ($D = 30$).

ties of the films prepared at dilution $D = 40$ and 50 were found. This is thought to be due to the stabilization in the evolution of the network structure.

The hydrogen content is well known to affect the apparent band gap of a-Si:H. H atoms remove dangling bonds and thus reduce tails increasing apparently the band gap. It was reported that the shift of E_g toward higher photon energies occurs with increasing H content [11–13]. Therefore, we can expect an increasing amount of hydrogen in the films with increasing dilution of hydrogen. Besides this, the increase of E_g at the amorphous-crystalline boundary is caused by the appearance of indirect gap (gap near 3.3 eV) of the crystalline silicon.

Therefore, we deduce that the samples prepared at $D \geq 30$ are polysilicon composed of grains and grain boundaries formed by amorphous Si and voids. Otherwise, polycrystalline films with voids are less homogeneous and therefore the optical results in Fig. 6, 7 extracted using a quasi-ideal film model can be interpreted only as effective. Further detailed analysis of optical properties of polysilicon thin films considered as a mixture of a-Si, c-Si and voids is necessary.

The following FTIR spectra analysis concerns the dilution series. According to the HATR geometry and refractive index relationships only bulk vibrational modes are recorded. FTIR spectra at wavenumbers $< 1300 \text{ cm}^{-1}$ are strongly influenced by the glass substrate and therefore often for the analysis used wagging absorption bands at $\sim 640 \text{ cm}^{-1}$ and bending bands at $\sim 850 \text{ cm}^{-1}$ are overlapped by the strong glass substrate absorbance.

Absorption bands of bulk stretching vibrational modes at $\sim 2000 \text{ cm}^{-1}$ assigned to silicon to hydrogen bonds give information about how H is bonded. Absorbance peaks at $\sim 2000 \text{ cm}^{-1}$ plotted in Fig. 10 were smoothed, baseline corrected and deconvoluted by least-squares fitting with Gaussian intensity distribution. Two broad overlapping stretching modes are present in the spectra: isolated SiH centred at $\sim 2000 \text{ cm}^{-1}$ and clustered SiH₂ at $\sim 2090 \text{ cm}^{-1}$. Presence of SiH_x, $x > 1$ is common for material with microvoids. A typical result of the deconvolution of the vibrational stretching band for the polycrystalline sample A 1371 is in Fig. 11.

The peak position of the monohydride SiH mode at $\sim 2000 \text{ cm}^{-1}$ for the dilution series is shifted towards higher wavenumbers as illustrated in Fig. 12. It was reported [14] that the observed shift can be due to the increasing hydrogen content and order in the Si network.

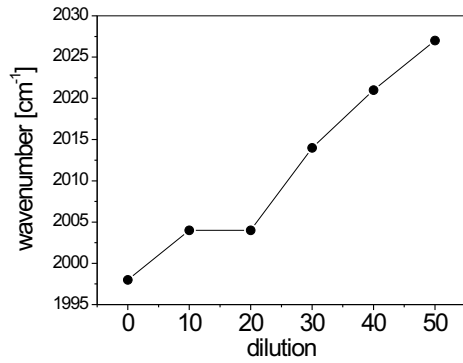


Fig. 12. Shift of the vibrational absorption peak at $\sim 2000 \text{ cm}^{-1}$ versus the dilution.

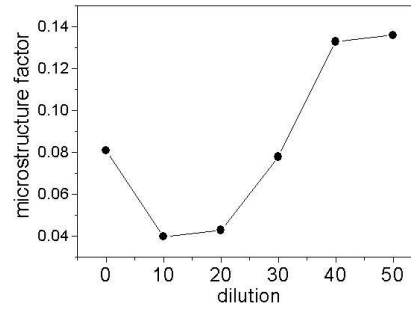


Fig. 13. Microstructure factor versus the hydrogen dilution of the SiH_4 .

Microstructure factor $v = \frac{\int I_{\text{SiH}_2}(\nu) d\nu}{\int I_{\text{SiH}_2}(\nu) d\nu + \int I_{\text{SiH}}(\nu) d\nu}$ is the ratio of the integral intensities of SiH and SiH_2 absorption bands (ν is the wavenumber). It expresses the ratio of SiH_2 bonds to the total bonded hydrogen [15]. The results depicted in Fig. 13 show that hydrogen is mainly bonded in the monohydride SiH but for $D > 20$ the contribution of the hydrogen in dihydride SiH_2 bonds increases thus remaining under the value of ~ 0.14 . Microstructure factor < 0.1 according to the reference [16] indicates a compact material with a low void fraction. Therefore, for the samples from the dilution series, the fraction of voids increases partly when D rises above ~ 20 , but still represents compact character of the films. This observation is supported by relatively high refractive index values (Fig. 6) and as it is shown in this plot, they decrease for the high-diluted samples as the void fraction increases.

4 Conclusion

Notable changes in the structural and optical properties of Si:H thin films prepared at the variable dilution were found. The crystallization becomes noticeable at the dilution $D \geq 30$ after the surface roughness reaches its maximum. The films from the dilution series prepared at $D \geq 30$ were nanometer grain-sized polycrystalline Si with grain boundaries passivated by hydrogen and voids. Grains in nanometer range exist within the surface features seen by AFM. FTIR results show primarily monohydride SiH bonding with increasing part of dihydride SiH_2 when the dilution rises. Dilution enables the refractive index and optical band gap engineering. The sample at $D \sim 30$ seems to be a proper candidate for photovoltaic applications.

The samples of the thickness series up to the value of $\sim 400 \text{ nm}$ prepared at the dilution $D = 20$ are found to remain within the amorphous regime with a negligible surface roughness, though while rising the thickness the band gap increases and the refractive index decreases.

Acknowledgement: This work was supported in part by the Slovak Grant Agency under grants No. 2/4105/04, No. 2/4100/04, No. 1/2454/2005 and by the Project of Research and Development LN00B084 of the Czech Ministry of Education, Youth and Sports. Dr V. Nádaždy at the

Institute of Physics, Slovak Academy of Sciences, Bratislava, Slovakia, is acknowledged for the sample preparation and Dr. M. Michalka at the International Laser Centre, Bratislava, Slovakia, for the AFM measurements.

References

- [1] C. R. Wronski, et al.: *Proc. of RIO 02 - World Climate & Energy Event*, Jan 2002, 67
- [2] R.C. Koval et al.: *Appl. Phys. Lett.* **75**, (1999) 1553
- [3] B. von Roedern: *NCPV and Solar Program Review Meeting 2003*, NREL/CD-520-33586, 552
- [4] V. Nádaždy et al.: *Phys. Rev. B* **66** (2002) 195211
- [5] J. Kočka et al.: *Proc. of 20th Int. Conf. Amorphous and Microcrystalline Semiconductors - ICAMS20*, Aug 2003, Paper No. Tu-C2/
- [6] A. Fejfar et al.: *Mat. Res. Soc. Symp. Proc.* **664** (2001) A 16.1.1.
- [7] A. J. M. M. van Zutphen et al.: *J. of Crystal Growth* **223** (2001) 332
- [8] V. Nádaždy: *private communication*
- [9] J. Müllerová, S. Jurečka, A. Kučerová: *Acta Phys. Slov.* **53** (2003) 111
- [10] S. Jurečka, J. Müllerová, E. Pinčík: *Proc. of the 10th Int. Workshop APCOM 2004*, June 2004, Častá – Píla, Slovakia, 108, ISBN 80-227-2073-9
- [11] Y. Ziegler et al.: *Solar Energy Materials and Solar Cells* **66** (2001) 413
- [12] H. Ch. Lee, S.I. Lee: *J. of the Korean Phys. Soc.* **39** (2001) S30
- [13] Y.B. Park et al.: *J. Phys. D: Appl. Phys.* **32** (1999) 1955
- [14] R. Ossikovski, B. Drevillon: *Phys. Rev. B* **54** (1996) 10530
- [15] Y. Ziegler et al.: *Solar Energy Materials and Solar Cells* **66** (2001) 413
- [16] B. Stannowski, R.E.I. Schropp: *Thin Solid Films* **383** (2001) 125